Journal of Power Sources 222 (2013) 123–128

Contents lists available at SciVerse ScienceDirect

Journal of Power Sources

journal homepage: www.elsevier.com/locate/jpowsour

The stability of lanthanum strontium vanadate for solid oxide fuel cells

Jong-Sung Park [b,*], Jing Luo [a], L. Adijanto [a], J.M. Vohs [a], R.J. Gorte [a]

[a] Department of Chemical and Biomolecular Engineering, University of Pennsylvania, Philadelphia, PA 19104, USA
[b] Department of Materials Science and Engineering, Myongji University, Yongin 449-728, Republic of Korea

HIGHLIGHTS

- Poor redox stability of the anode based on $La_{0.7}Sr_{0.3}VO_3$ (LSV) with a Pd catalyst.
- Deactivation of a Pd-catalyst due to the molten phase from LSV in oxidized condition.
- Improvement of the redox stability using the V-deficient LSV.

ARTICLE INFO

Article history:
Received 3 July 2012
Received in revised form
28 August 2012
Accepted 29 August 2012
Available online 7 September 2012

Keywords:
Solid oxide fuel cells
Composite anode
Strontium vanadate
Lanthanum vanadate
Redox stability

ABSTRACT

The deactivation upon oxidative treatments of solid oxide fuel cell (SOFC) anodes based on $La_{0.7}Sr_{0.3}VO_{3.85}$ with a Pd/ceria catalyst is examined using electrodes formed by infiltration of $La_{0.7}Sr_{0.3}VO_{3.85}$, Pd, and ceria into porous yttria-stabilized zirconia (YSZ). Based on XRD results, performance measurements of cells made with varying La:Sr:V ratios, and Pd dispersion measurements using CO adsorption, we conclude that $La_{0.7}Sr_{0.3}VO_{3.85}$ is kinetically unstable upon reduction-oxidation treatments at 973 K, forming molten, strontium–vanadate phases that partially cover the catalytic component. Deactivation can be minimized using V-deficient compositions.

1. Introduction

Although state-of-the-art, solid oxide fuel cells (SOFC) are usually based on a composite of Ni and the electrolyte material, typically yttria-stabilized zirconia (YSZ) [1,2], there would be significant advantages in replacing the Ni with a ceramic conductor if comparable electrochemical performance could be achieved. Ceramic conductors would likely exhibit improved redox stability, better tolerance to sulfur poisoning, and better resistance toward coking in the presence of hydrocarbons [3,4]. Finding ceramic replacements for Ni, however, is challenging since the ceramic must remain stable and exhibit high electronic conductivity over the wide $P(O_2)$ range that can exist in the anode compartment. The ceramic anode must also resist reaction with the electrolyte at temperatures required for cell fabrication and exhibit catalytic activity for oxidation of the fuel. Finally, electrode fracture can be a problem if the electrode expands or contracts relative to the electrolyte due to differences in the Coefficient of Thermal Expansion (CTE) or due to changes in volume due to reduction.

The problems of solid-state reaction and differences in the relative expansion with respect to the electrolyte can be addressed by using infiltration methods to prepare the cell electrodes [5,6]. This synthesis procedure involves making a porous scaffold of the electrolyte material together with the dense electrolyte, then infiltrating the electronic conductor and a catalyst into the pores of the scaffold [7]. Contact between the electrolyte and electrode materials need not occur until after all high-temperature processes have been completed. The mechanical properties of composites formed by infiltration, such as CTE, are largely determined by the scaffold material, which is the same as that used for the electrolyte [5]. A number of different ceramic anodes have been prepared in this way, including ones based on $La_{0.8}Sr_{0.2}Cr_{0.5}Mn_{0.5}O_3$ (LSCM) [7,8], $La_{0.3}Sr_{0.7}TiO_3$ (LST) [9–11], $SrMoO_3$ [12], $NaWO_3$ [13], $La_{0.7}Sr_{0.3}VO_{3.85}$ [14,15], and $Ce_{0.7}Sr_{0.3}VO_{3.85}$ [13,16]. Because none of these oxides has catalytic activity approaching that of Ni for oxidation reactions, it is necessary to also add a catalytic metal, in dopant quantities, in order to reduce polarization losses [14,17].

* Corresponding author. Tel.: +82 31 330 6467; fax: +82 31 330 6469.
E-mail addresses: jspark.phd@mju.ac.kr, jspark.phd@gmail.com (J.-S. Park).

0378-7753/$ – see front matter © 2012 Elsevier B.V. All rights reserved.
http://dx.doi.org/10.1016/j.jpowsour.2012.08.084

Among the oxides tested in our laboratory, the vanadates exhibit some of the best overall properties. Unlike $SrMoO_3$ [18], vanadates undergo reduction to their conductive phases at relatively high $P(O_2)$, similar to that required for reduction of NiO [19]; and they cannot be over reduced at lower $P(O_2)$, as in the case of $NaWO_3$. They have electronic conductivities that are at least an order of magnitude higher than that of LSCM or LST under practical SOFC anode conditions, with bulk conductivities reported to be well over 100 S cm^{-1} [20]. In an earlier study, we showed that the conductivity of an $La_{0.7}Sr_{0.3}VO_{3.85}$-YSZ composite with only 10-vol.% $La_{0.7}Sr_{0.3}VO_{3.85}$ is 1 S cm^{-1} at 973 K, sufficiently high to make ohmic losses in the anode composite negligible [14]. As with other ceramic conductors, low anode polarization losses are only observed after the addition of transition-metal dopants [7,14], demonstrating that $La_{0.7}Sr_{0.3}VO_{3.85}$ is not a good electrocatalyst.

Unfortunately, fuel cells made from $La_{0.7}Sr_{0.3}VO_{3.85}$-YSZ, with 0.5-vol.% Pd and 2.3-vol.% ceria as the catalyst, exhibited large increases in their polarization losses after a single oxidation–reduction cycle [14]. Since this treatment did not change the ohmic losses significantly, it would appear that the catalytic component of the electrode was lost. Although catalyst sintering can be a problem with low metal loadings after high-temperature treatments, no comparable losses were observed following similar treatments with anodes based on LSCM [7] or LST [11] and oxidation cycles should actually improve the dispersion of the Pd catalyst [21]. Interestingly, the use of a V-deficient vanadate, $La_{0.7}Sr_{0.3}V_{0.9}O_{3.85-\delta}$, minimized the loss in performance following this redox treatment [14,22]. Because the ability to periodically oxidize the anode is a primary advantage for using ceramics, it is important to understand the reasons behind the deactivation of LSV-based electrodes and to determine what can be done to prevent deactivation from occurring.

In the present study, we investigated the deactivation of the vanadate-based anodes in more detail. We discovered that deactivation upon redox cycling of $La_{0.7}Sr_{0.3}VO_{3.85-\delta}$-YSZ electrodes is due to the instability of the vanadate, which results in the formation of small amounts of a molten phase, $Sr_2V_{2+\chi}O_{7+\delta}$ ($0 < \chi < 1.02$) that covers the Pd catalyst. The use of V-deficient LSV minimizes the formation of the molten phase, so that the electrode performance is maintained.

2. Experimental procedure

The SOFC button cells in this study were prepared using the same methods described in previous work [14]. Briefly, the first step involved preparation of YSZ wafers, each having a dense layer, 70–80-μm in thickness, with 40-μm porous layers on both sides. These were fabricated by tape casting and lamination, using graphite pore formers for the porous layers. The wafers were calcined to 1773 K before the electrode components were added to the porous layers by infiltration. The outside layers had a porosity of approximately 65 vol.%, with a sponge-like structure and typical pore dimensions between 1 and 3-μm. The diameter of the dense layer was 1 cm but the diameter of the porous regions used for both electrodes was only 0.67 cm. The $La_{0.8}Sr_{0.2}FeO_3$ (LSF)-YSZ cathodes were prepared by infiltration into one of the porous layers using the nitrate salts and procedures described in other papers [23]. The final loading of LSF was 20 vol.% and the final calcination step was 1123 K.

The anodes were prepared by infiltration of the $La_xSr_yV_zO_\delta$ ($L_xS_yV_z$) phase into the porous layer opposite the cathode. The precursor solutions for synthesizing $L_xS_yV_z$ used $La(NO_3)_3 \cdot 6H_2O$ (99.9%, Alfa Aesar), $Sr(NO_3)_2$ (99.9%, Alfa Aesar), and NH_4VO_3 (99%, Alfa Aesar) in distilled water, with the addition of citric acid (100.7%, Fisher Scientific) in the amount of 1 mol per mole of metal cations. After infiltration of the salt solutions, the $L_xS_yV_z$ phase was formed by calcination at 973 K in air. The loading of the $L_xS_yV_z$ phase was 10-vol.% in all cases except the $L_1S_0V_z$; we used 20-vol.% of $L_1S_0V_z$ due to the lower conductivity of the undoped material [20]. Next, CeO_2 (1 M $Ce(NO_3)_3$, Alfa Aesar, 99.5%) and Pd (0.45 M Tetraammine palladium(II) nitrate solution, Alfa Aesar, 99.9%) were infiltrated into the $L_xS_yV_z$-YSZ, followed by heating in air to 723 K, to achieve a loading of a 2.8 vol.% CeO_2 and 0.5 vol.% Pd. In one case, Pt (0.24 M Tetraammine platinum (II) nitrate solution, Alfa Aesar, 99.9%) was used in place of Pd.

To measure performance, the cells were mounted onto an alumina tube using a ceramic adhesive (Ceramabond 552-VFG, Aremco); Ag wire and Ag paste (#05063-AB, SPI supplies) were used for current collection on both sides. While the cathode was simply exposed to the atmosphere, humidified (3% H_2O) H_2 was passed over the anode at a flow rate of approximately 1 mLs^{-1}. The *V–i* polarization curves and impedance spectra were measured using a Gamry Instruments potentiostat. Impedance spectra were measured with a −0.1-V bias from the open circuit voltage (OCV), in the frequency range from 100 kHz to 0.01 Hz, with a 20-mV AC perturbation.

Prior to the initial electrochemical measurements, care was taken to avoid heating the combined catalyst and $L_xS_yV_z$ phase above 723 K in air. For the electrochemical tests, the anodes were heated from room temperature to their operating temperature in humidified H_2. In order to see the impact of oxidizing these two components together, the following experiment was performed. After testing the electrodes at 973 K in humidified H_2, the anode compartment was first flushed with He, then exposed to flowing air for 1 h at 973 K, and again flushed with He before testing in humidified H_2.

Physical characterization of the anode composites was carried out by scanning electron microscopy (SEM) (FEI Quanta 600 ESEM) and X-ray diffraction (XRD) using Cu K_α radiation. To determine the Pd surface areas (Pd dispersion), CO adsorption was performed on composite slabs (4 mm × 4 mm × 15 mm) prepared using identical procedures to that used in preparing electrodes, except that no ceria was added. For measurements on samples referred to as "oxidized", the Pd was reduced at only 723 K. CO adsorption uptakes were measured volumetrically at room temperature and dispersion was calculated by assuming a stoichiometry of one CO molecule per surface Pd. Pure $L_xS_yV_z$ powders were prepared for some of the XRD studies.

3. Results and discussion

The electrochemical performance of cells with $L_{0.7}S_{0.3}V_1$-YSZ composite anodes exposed to humidified H_2, with identical cathodes and electrolytes, has been discussed in detail elsewhere [14]. At 973 K, there was sufficient conductivity with 10-vol.% $L_{0.7}S_{0.3}V_1$ to ensure that ohmic losses in the cell were equal to that expected from the 80-μm YSZ electrolyte, 0.4 Ω cm^2. However, the non-ohmic losses were strongly affected by the addition of the CeO_2 and Pd catalysts. In the absence of an added catalyst, the cells exhibited large non-ohmic losses, ~2.5 Ω cm^2, and a maximum power density of only 90 mW cm^{-2}. Addition of a Pd/ceria catalyst decreased the non-ohmic losses to ~0.2 Ω cm^2 and increased the maximum power density to 470 mW cm^{-2}. Although Pd was sufficient for decreasing the non-ohmic losses in the cell without ceria, the addition of both ceria and Pd led to better performance at high current densities [24]. The open-circuit voltage (OCV) was unaffected by the addition of the Pd/ceria catalyst.

Fig. 1 shows *V–i* curves and impedance spectra for a similar cell used in the present study, before and after treatment in air. The anode in this cell again consisted of 10-vol.% $L_{0.7}S_{0.3}V_1$, 2.8-vol.%

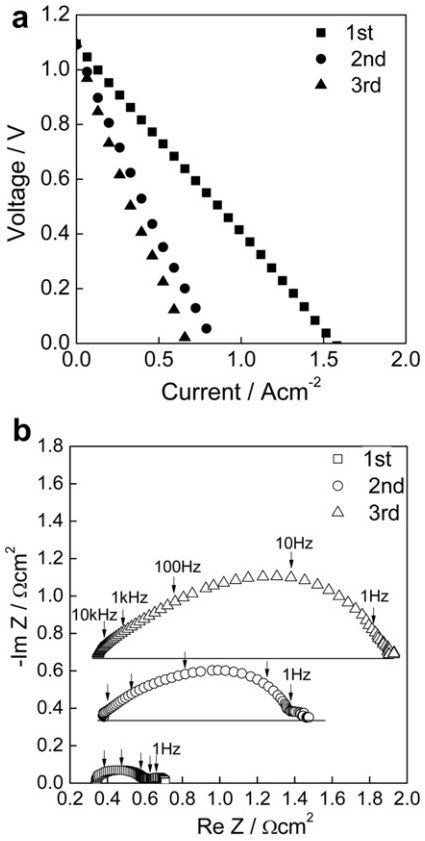

Fig. 1. (a) *V*–*i* polarization curves and (b) impedance spectra at 973 K for an SOFC with an anode composition of 10-vol.% $L_{0.7}S_{0.3}V_1$, 2.8-vol.% CeO_2, and 0.5-vol.% Pd catalyst, in a porous YSZ scaffold, initially and after one and two redox cycles.

CeO_2, and 0.5-vol.% Pd in the porous YSZ scaffold, but the electrolyte was only 70-μm thick. Initially, the maximum power density was 440 mW cm^{-2} and the impedance spectrum showed that the ohmic losses, associated with the electrolyte, contributed approximately 0.35 Ω cm^2 to the total cell resistance of 0.7 Ω cm^2. The non-ohmic losses in this cell, 0.35 Ω cm^2, were slightly higher than those observed in our previous study but this may be partially due to variations in the LSF-YSZ cathode performance, which typically exhibits non-ohmic resistances between 0.1 and 0.2 Ω cm^2 [23]. Prior to the oxidation treatment, the non-ohmic resistance of the anode must have been less than 0.25 Ω cm^2. However, treatment of the anode by oxidation in air for 1 h at 973 K decreased its performance in humidified H_2 dramatically, without changing the ohmic resistance of the cell. After a single anode oxidation cycle, the non-ohmic resistance of the cell increased to 1.1 Ω cm^2, with a concomitant decrease in the maximum power density to 200 mW cm^{-2}. A second oxidation step increased the non-ohmic losses even further, to 1.61 Ω cm^2.

In order to understand the reasons for the strong sensitivity of the anode to oxidation treatments, we examined a series of cells that were identical except for the anode compositions. The data for this series are summarized in Table 1, along with the results from the cell used in Fig. 1 for comparison. Because the vanadate phase in each of these cells had been heated to 973 K in air together with the YSZ scaffold prior to the addition of the Pd/ceria catalyst, we focused initially on the effects of oxidation on interactions between the vanadate phase and the Pd/ceria catalyst. Because Pd is known to react with some perovskites and could be lost to the electrode surface through such a reaction [25,26], we replaced the 0.5-vol.% Pd with 0.5-vol.% Pt. Pt can provide similar catalytic activity to the anode [17,24] but is not expected to form perovskites in the same manner as Pd. As shown in Table 1, both the initial performance and the deactivation characteristics upon oxidation were even worse for the Pt-containing cell as was observed for the cell made with Pd. The initial non-ohmic resistance of the Pt cell was 0.4 Ω cm^2 prior to oxidation treatments and increased to 2.8 Ω cm^2 after oxidation cycles. The lower performance with Pt may be due to the fact that Pt is not as easily re-dispersed by oxidation [21]. In any case, the large increase in the non-ohmic losses for cells made with both Pt and Pd implies that incorporation of metals into the oxide lattice is unlikely to be the reason for the lost performance.

Because the performance of cells has been shown to degrade with Pd sintering [27], we examined a cell made with 1.5-vol.% Pd, a Pd loading three times higher than that used in the cells in Fig. 1. The initial non-ohmic impedance of this cell as measured by the impedance spectrum was somewhat better than that of the cell with lower Pd loading, 0.3 Ω cm^2 versus 0.35 Ω cm^2, and the degradation after three oxidation cycles was less, 0.7 Ω cm^2 versus 2.5 Ω cm^2. The fact that the degradation was less with the added Pd is additional evidence that deactivation is associated with the catalytic function; however, there was still a significant, unacceptable loss in performance upon oxidation, even with the higher Pd loading.

Finally, we prepared cells with various oxide compositions, varying the La:Sr:V ratios, but still including 2.8-vol.% ceria and 0.5-vol.% Pd. The cell made with $L_1S_0V_1$ (undoped $LaVO_4$) showed a lower initial power density (295 mW cm^{-2}) and slightly higher non-ohmic impedance (0.44 Ω cm^2) than cells made with $L_{0.7}S_{0.3}V_1$, probably because the conductivity of the $LaVO_3$ is low [28]. Even with 30-wt% $L_1S_0V_1$ in porous YSZ, the conductivity was only 0.1 S cm^{-1} [28], a value that is barely adequate for this application.

Table 1
Fuel cell performances before and after redox cycles for various anode compositions. The anodes were all YSZ composites formed infiltration.

Anode composition[a]	Initial			After 2nd oxidation		
	ASR(Ω cm^2)		Max. Power (mW cm^{-2})	ASR(Ω cm^2)		Max. Power (mW cm^{-2})
	Ohmic	Non-ohmic		Ohmic	Non-ohmic	
$L_{0.7}S_{0.3}V_1$ + 0.5 vol.% Pd	0.34	0.37	435	0.35	1.57	165
$L_{0.7}S_{0.3}V_1$ + 0.5 vol.% Pt	0.41	0.40	420	0.44	2.78	90
$L_{0.7}S_{0.3}V_1$ + 1.5 vol.% Pd	0.48	0.29	460	0.52	0.70	280
$L_{0.7}S_{0.3}V_{0.9}$ + 0.5 vol.% Pd	0.48	0.36	450	0.50	0.43	370
$L_{0.7}S_{0.3}V_{0.8}$ + 0.5 vol.% Pd	0.39	0.33	420	0.36	0.39	390
$L_1S_0V_1$ + 0.5 vol.% Pd	0.34	0.44	295	0.32	0.52	295
$L_1S_0V_{0.9}$ + 0.5 vol.% Pd	0.47	0.45	280	0.43	0.46	290
$L_0S_1V_1$ + 0.5 vol.% Pd	0.47	0.48	290	0.42	0.70	220
$L_0S_1V_{0.9}$ + 0.5 vol.% Pd	0.67	0.95	195	0.59	1.2	155

[a] All of anodes had 2.8 vol.% CeO_2.

What is more interesting is that the maximum power density for the cell did not change after redox cycling. The cell prepared with the V-deficient analog, $L_1S_0V_{0.9}$, was also unaffected by redox cycling, even showing a slight increase in the maximum power density. By contrast, cells made from $L_0S_1V_1$ ($Sr_2V_2O_7$) and its V-deficient analog $L_0S_1V_{0.9}$ did show significant deactivation after redox cycling. The initial performance is again lower, in part because this material is difficult to reduce [15]; but an additional performance decline occurred after redox cycling. These data indicate that the loss of performance is associated with a strontium vanadate phase, not with lanthanum vanadate. Furthermore, vanadium poisoning by itself does not appear to be important.

To confirm that deactivation of cells made with $L_{0.7}S_{0.3}V_1$ is associated with loss of active Pd and that loss of Pd activity with the V-deficient material, $L_{0.7}S_{0.3}V_{0.9}$, is less, we measured room-temperature CO adsorption uptakes on samples with 0.5-vol.% Pd, before and after oxidation treatment at 973 K (It was still necessary to reduce the Pd in order to perform CO adsorption but reduction was carried out at 723 K to avoid sintering of the metallic Pd.) As shown in Table 2, the initial Pd dispersion on both samples was near 1%, which corresponds to an average Pd particle size of 100 nm. This is a low value for the Pd dispersion of a supported catalyst but not entirely unreasonable given the low surface area of the electrode and the relatively high reduction temperature of 973 K. After redox cycling, the dispersion of the Pd in the $L_{0.7}S_{0.3}V_1$ composite was only 0.1%, a factor of 10 lower than the starting dispersion, while the dispersion on the composite with $L_{0.7}S_{0.3}V_{0.9}$ was significantly higher, 0.49%. If this loss of Pd surface area were due to growth of the Pd particles, the particles in the $L_{0.7}S_{0.3}V_1$ composite would be very large, nearly 1 μm in diameter.

Since it should be easy to observe Pd particles that are larger than 100 nm by SEM, we examined samples that were identical to those used in the adsorption measurements of Table 2. Because reduction of $L_{0.7}S_{0.3}V_1$ resulted in such a rough surface that the Pd could not be distinguished [13], we show micrographs only for samples treated in air for 2 h at 973 K. As shown in Fig. 2 the Pd particles were easily visible on both the $L_{0.7}S_{0.3}V_1$ and the $L_{0.7}S_{0.3}V_{0.9}$ samples. The fact that the observed features are due to Pd was also confirmed by EDS analysis. For both the $L_{0.7}S_{0.3}V_1$ and the $L_{0.7}S_{0.3}V_{0.9}$ samples, the Pd particles sizes were between 20 and 30 nm in diameter, with no major difference between the samples. There was no evidence for particles greater than 100 nm in size, suggesting that the low dispersion is not due to the Pd existing as large particles.

To better understand the effect of redox treatments on the $L_xS_yV_z$ phases, more detailed XRD measurements were performed on the $L_{0.7}S_{0.3}V_1$ and $L_{0.7}S_{0.3}V_{0.9}$ powders, before and after redox treatments. Fig. 3a shows the patterns after normal calcination in air at 973 K for 1 h, along with reference patterns for the monoclinic monazite structure of $LaVO_4$ (JCPDS card No.50-0367) and for $Sr_3V_2O_8$ (JCPDS card No.81-1844). The pattern for $L_{0.7}S_{0.3}V_1$ agrees well with that of $LaVO_4$. An earlier study of XRD lattice parameters as a function of Sr content also indicated that Sr is incorporated into the lattice at this composition [28]. The pattern for $L_{0.7}S_{0.3}V_{0.9}$ shows a significant contribution from $Sr_3V_2O_8$. After reduction in flowing humidified H_2 at 973 K for 1 h, Fig. 3b, the XRD indicate that both materials form the perovskite structure, $LaVO_3$, with only minor quantities of the impurity phases, $Sr_3V_2O_8$, which is relatively difficult to reduce, and La_4SrO_7 (JCPDS card No.22-1430). The decreased intensities for the impurity phases may imply that the perovskite structure is more tolerant than the monoclinic monazite structure for changes in composition, although we cannot rule out the presence of small crystallites or amorphous material.

The most informative result was obtained when the reduced $L_{0.7}S_{0.3}V_1$ and $L_{0.7}S_{0.3}V_{0.9}$ samples were re-oxidized for 1 h in air and then reduced again in humidified H_2 at 973 K. The XRD patterns for these two samples, along with patterns for $LaVO_4$ and $Sr_2V_2O_7$, reduced in humidified H_2 at 973 K for 1 h, are shown in Fig. 4. Because $Sr_2V_2O_7$ is only partially reduced to $SrVO_3$ at 973 K, there is a significant peak associated with $Sr_3V_2O_8$ in the XRD pattern of this sample. It is surprising that, after this redox treatment, the reduced $L_{0.7}S_{0.3}V_1$ shows two peaks at 32.95 and 40.65° 2θ, while the V-deficient $L_{0.7}S_{0.3}V_{0.9}$ material remained mostly single phase. The peak at 32.95° 2θ in the pattern for $L_{0.7}S_{0.3}V_1$ indicates that this material is not phase stable to redox cycling and that $SrVO_3$ is formed, even though this was not observed after the initial calcination and reduction. Interestingly, the $L_{0.7}S_{0.3}V_{0.9}$ sample exhibited much less of this phase.

As shown in Fig. 5, the phase diagram for the $SrO–V_2O_5$ system exhibits several phases that have low melting temperatures, SrV_2O_6

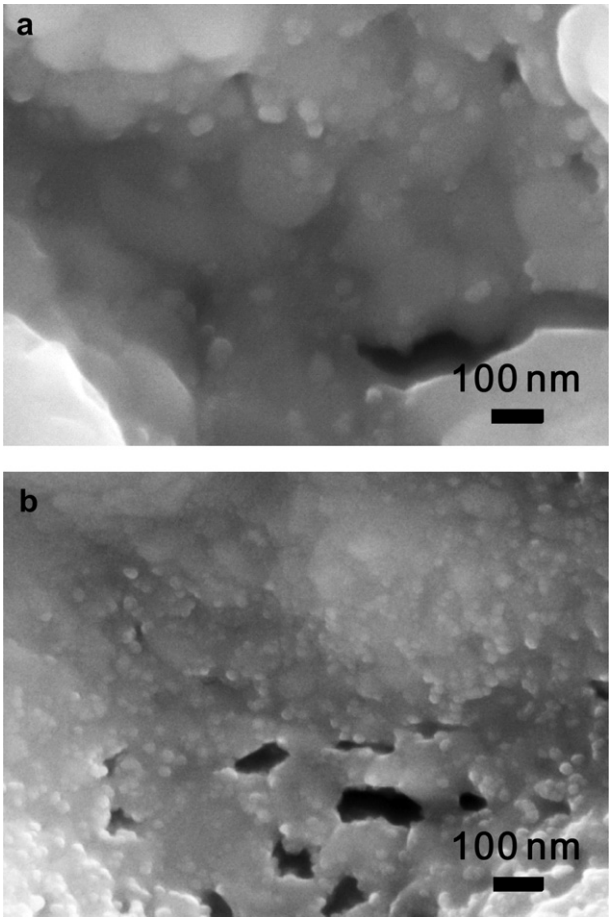

Fig. 2. SEM images of Pd particles on (a) $L_{0.7}S_{0.3}V_1$ and (b) $L_{0.7}S_{0.3}V_{0.9}$ after heat treatment at 973 K for 2 h in air without reduction.

Table 2
Pd dispersions measured by CO chemisorption on composite slabs made by infiltration of 0.5-vol.% Pd and either 10-vol.% $L_{0.7}S_{0.3}V_1$ or $L_{0.7}S_{0.3}V_{0.9}$ in the YSZ slabs. Initial results were obtained immediately after reduction at 973 K, prior to any oxidation steps above 723 K. The results after redox were obtained on the same samples after oxidation in air at 973 K, followed by reduction in dry H_2 at 723 K. The Pd particle diameters were calculated assuming spherical particles with one CO adsorbed on each surface Pd.

	$L_{0.7}S_{0.3}V_1$		$L_{0.7}S_{0.3}V_{0.9}$	
	Dispersion (%)	Particle size (nm)	Dispersion (%)	Particle size (nm)
Initial	1.14	100	1.01	110
Redox	0.10	1130	0.49	230

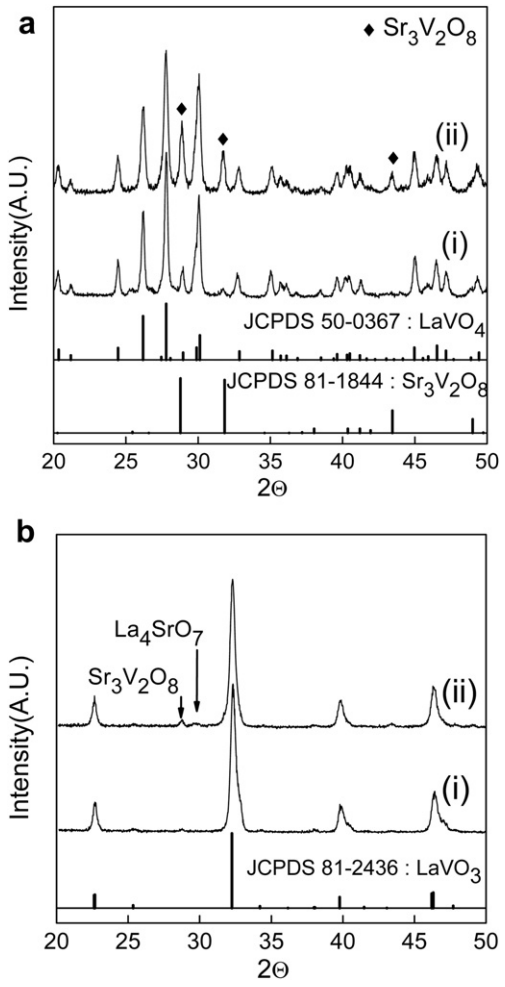

Fig. 3. (a) XRD patterns after calcination to 973 K in air of the following materials: (i) $L_{0.7}S_{0.3}V_1$ and (ii) $L_{0.7}S_{0.3}V_{0.9}$ and (b) XRD patterns after reduction at 973 K in humidified H_2 of the following materials: (i) $L_{0.7}S_{0.3}V_1$ and (ii) $L_{0.7}S_{0.3}V_{0.9}$.

(918 K) and a eutectic mixture of $Sr_2V_2O_7$ and SrV_2O_6 with a melting temperature of 803 K [29]. Therefore, the presence of $SrVO_3$ in the XRD pattern of $L_{0.7}S_{0.3}V_1$ after redox cycling implies that liquid phases could be formed. We suggest that formation of these liquid phases is causing the deactivation of electrodes based on

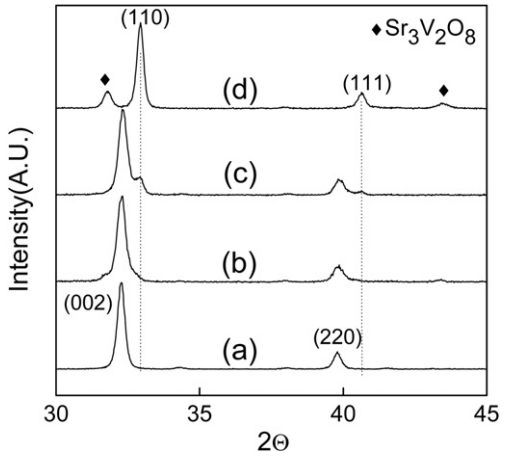

Fig. 4. XRD patterns of various oxide compositions after one redox cycle at 973 K: (a) $L_1S_0V_1$ (b) $L_{0.7}S_{0.3}V_{0.9}$, (c) $L_{0.7}S_{0.3}V_1$ and (d) $L_0S_1V_1$.

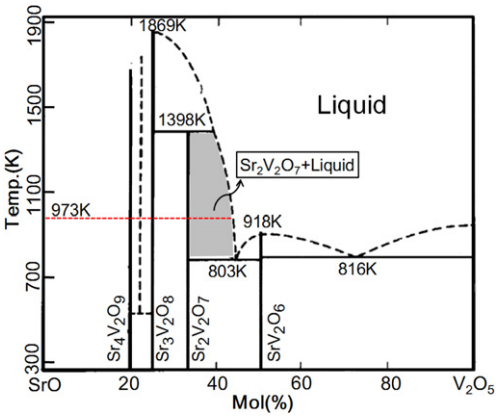

Fig. 5. Phase diagram for the SrO–V_2O_5 system [29].

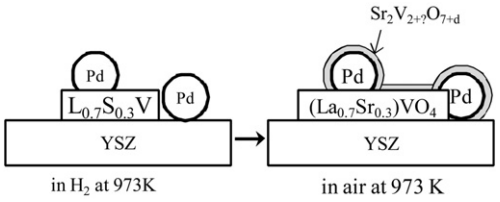

Fig. 6. A schematic of the proposed mechanism for deactivation of the Pd catalyst following redox cycling of electrodes based on $La_{0.7}Sr_{0.3}O_{3.85}$.

$L_{0.7}S_{0.3}V_1$-YSZ composites. While the amount of molten material associated with the $L_{0.7}S_{0.3}V_1$-YSZ composite following calcination is a small fraction of the total amount of ceramic material in the electrode, it is apparently catastrophic for the catalytic component of the electrode. For Pd in particular, the amount of molten material is likely comparable to the Pd content, so that the Pd catalyst can easily be covered, as shown schematically in Fig. 6.

Since $La_{0.7}Sr_{0.3}VO_{3.85}$ has been shown to be stable under oxidizing conditions [15,20,28], the formation of strontium–vanadate phases following redox treatments must be a kinetic limitation. There must be a separation of phases upon reduction that cannot be restored by simple heating in air to 973 K for short times. Even though the amounts of the new phases are relatively small and do not affect the conductivity of the electrode, they are sufficient to poison the catalytic component. Fortunately, it appears to be possible to minimize separation of phases and poisoning of the catalyst by reducing the vanadium content of the initial materials.

4. Conclusions

$La_{0.7}Sr_{0.3}VO_{3.85}$ is shown to be kinetically unstable toward redox treatment, forming small amounts of a molten, strontium–vanadate phase that is capable of deactivating catalytic components in SOFC anodes. Deactivation of the catalytic components can be minimized through the use of vanadium-deficient compositions.

Acknowledgment

This work was funded by the U.S. Department of Energy's Hydrogen Fuel Initiative (Grant DE-FG02-05ER15721).

References

[1] N.Q. Minh, J. Am. Ceram Soc. 76 (1993) 563–588.
[2] C.W. Sun, U. Stimming, J. Power Sources 171 (2007) 247–260.
[3] D. Sarantaridis, A. Atkinson, Fuel Cells 7 (2007) 246–258.

[4] A. Atkinson, S. Barnett, R.J. Gorte, J.T.S. Irvine, A.J. McEvoy, M. Mogensen, S.C. Singhal, J. Vohs, Nat. Mater. 3 (2004) 17–27.
[5] J.M. Vohs, R.J. Gorte, Adv. Mater. 21 (2009) 943–956.
[6] H.P. He, Y.Y. Huang, J. Regal, M. Boaro, J.M. Vohs, R.J. Gorte, J. Am. Ceram. Soc. 87 (2004) 331–336.
[7] G. Kim, G. Corre, J.T.S. Irvine, J.M. Vohs, R.J. Gorte, Electrochem. Solid St. 11 (2008) B16–B19.
[8] J. Peña-Martínez, D. Marrero-López, J.C. Ruiz-Morales, C. Savaniu, P. Núñez, J.T.S. Irvine, Chem. Mater. 18 (2006) 1001–1006.
[9] G. Kim, M.D. Gross, W. Wang, J.M. Vohs, R.J. Gorte, J. Electrochem. Soc. 155 (2008) B360–B366.
[10] X. Sun, S. Wang, Z. Wang, X. Ye, T. Wen, F. Huang, J. Power Sources 183 (2008) 114–117.
[11] S. Lee, G. Kim, J.M. Vohs, R.J. Gorte, J. Electrochem. Soc. 155 (2008) B1179–B1183.
[12] B.H. Smith, M.D. Gross, Electrochem. Solid-State Lett. 14 (2011) B1–B5.
[13] L. Adijanto, R. Küngas, J. Park, J.M. Vohs, R.J. Gorte, Int. J. Hyd. Energ. 36 (2011) 15722–15730.
[14] J.S. Park, I.D. Hasson, M.D. Gross, C. Chen, J.M. Vohs, R.J. Gorte, J. Power Sources 196 (2011) 7488–7494.
[15] Z. Cheng, S.W. Zha, L. Aguilar, M.L. Liu, Solid State Ionics 176 (2005) 1921–1928.
[16] C.T.G. Petit, R. Lan, P.I. Cowin, J.T.S. Irvine, S. Tao, J. Mater. Chem. 21 (2011) 525–531.
[17] J.-S. Kim, V.V. Nair, J.M. Vohs, R.J. Gorte, Scripta Materialia 65 (2011) 90–95.
[18] I. Baldychev, A. Javadekar, D.J. Buttrey, J.M. Vohs, R.J. Gorte, Appl. Catal. A: Gen. 394 (2011) 287–293.
[19] P.R. Shah, M.M. Khader, J.M. Vohs, R.J. Gorte, J. Phys. Chem. C 112 (2008) 2613–2617.
[20] S.Q. Hui, A. Petric, Solid State Ionics 143 (2001) 275–283.
[21] K. Narui, H. Yata, K. Furuta, A. Nishida, Y. Kohtoku, T. Matsuzaki, Appl. Catal. A: Gen. 179 (1999) 165–173.
[22] N.M. Vo, M.D. Gross, J. Electrochem. Soc. 159 (2012) B641–B646.
[23] F. Bidrawn, G. Kim, N. Aramrueang, J.M. Vohs, R.J. Gorte, J. Power Sources 195 (2010) 720–728.
[24] G. Kim, S. Lee, J.Y. Shin, G. Corre, J.T.S. Irvine, J.M. Vohs, R.J. Gorte, Electrochem. Solid St. 12 (2009) B48–B52.
[25] U.G. Singh, J. Li, J.W. Bennett, A.M. Rappe, R. Seshadri, S.L. Scott, J. Catal. 249 (2007) 349–358.
[26] M.B. Bellakki, T. Baidya, C. Shivakumara, N.Y. Vasanthacharya, M.S. Hegde, G. Madras, Appl. Catal. B-Environ. 84 (2008) 474–481.
[27] J.-S. Kim, N.L. Wieder, A.J. Abraham, M. Cargnello, P. Fornasiero, R.J. Gorte, J.M. Vohs, J. Electrochem. Soc. 158 (2011) B596–B600.
[28] L. Adijanto, V. Balaji Padmanabhan, K.J. Holmes, R.J. Gorte, J.M. Vohs, J. Solid State Chem. 190 (2012) 12–17.
[29] J.J. Brown, J. Am. Ceram. Soc. 55 (1972) 500–503.